ELSEVIER

Catalysis Today 51 (1999) 93–101

CATALYSIS TODAY

# Rhodium-oxide species formed on progressive oxidation of rhodium clusters dispersed on alumina

Chin-Pei Hwang[a], Chuin-Tih Yeh[a,*], Qiming Zhu[b]

[a]Department of Chemistry, National Tsing-Hua University, Hsinchu, Taiwan 30043, China
[b]Department of Chemistry, Tsinghua University, Beijing 100084, China

**Abstract**

Samples of rhodium crystallites finely dispersed on alumina were prepared by impregnating an alumina support with different amounts of rhodium chloride. Reduced samples were oxidized at different temperatures ($T_o$) in air and the oxidized rhodium crystallites were characterized by the temperature-programmed reduction technique (TPR). According to the reduction peaks found by TPR, five kinds of oxidation products, i.e., oxygen-chemisorbed rhodium ($RhO_c$), surface rhodium-oxide ($Rh_sO$), bulk rhodium-oxides ($RhO_x$), rhodium-oxides interacting with support ($Rh_iO_x$) and rhodium aluminate [$Rh(AlO_2)_y$], have been progressively formed on increasing $T_o$ temperature. The abundance of these products on oxidized samples varied with $T_o$ temperature and the dispersion of supported rhodium crystallites. Rhodium atoms in the $Rh(AlO_2)_y$ structure, formed on severe oxidation conditions, would segregate from the bulk to the surface of alumina upon reductions at temperature above 750°C. © 1999 Elsevier Science B.V. All rights reserved.

*Keywords:* Rhodium-oxides; Alumina; Oxidation; Reduction

## 1. Introduction

$Rh/Al_2O_3$ is one of the active catalysts for oxidations of ammonia and carbon monoxide, the elimination of nitric oxide and the conversion of synthesis gas to oxygenates [1]. In oxidative environments, rhodium atoms dispersed on alumina tended to be oxidized into oxide forms of various compositions, i.e.,

$$2Rh/Al_2O_3 + xO_2 \leftrightarrow 2RhO_x/Al_2O_3 \quad (1)$$

Species of $Rh_2O$ [2], RhO [3], $Rh_2O_3$ [2,4–8], and $RhO_2$ [8,9] have been suggested to exist on oxidized rhodium catalysts (Table 1). The $RhO_x$ species formed on supported rhodium samples varied significantly with the properties of support. Munoz et al. [2] distinguished two rhodium oxide states, i.e., Rh(I), Rh(III), on $TiO_2$ support with a combination of XPS (X-ray photoelectron spectroscopy) and TPR (temperature-programmed reduction) techniques. Also based on XPS study, both Schmidt and coworker [6] and Carpenter [7] demonstrated that Rh(III) prevailed on alumina and silica supports. Using the combined techniques of the high resolution electron microscopy (HREM) and the $O_2$-uptake measurement, Datye and coworkers [3] found that a RhO intermediate state existed before the formation of $Rh_2O_3$ during oxidation of $Rh/SiO_2$ and $Rh/TiO_2$ samples. Sachtler and coworkers [8] reported that oxidation states of rhodium on Rh/NaY samples

---

*Corresponding author. Fax: +886-3-5711082; e-mail: ctyeh@chem.nthu.edu.tw

PII: S0920-5861(99)00011-5

Table 1
Rhodium oxide species suggested in the literature

| Sample | Oxidation condition | | Method | Oxide states ($RhO_x$) | Reference |
|---|---|---|---|---|---|
| | Temperature (°C) | Flowing gas | | | |
| 2.5% $Rh/TiO_2$ | 25 | $O_2$ | XPS/TPR | Rh(I) | Munoz et al. [2] |
| | 500 | | | Rh(I), Rh(III) | |
| $Rh/SiO_2$ | 500 | Air | XPS | Rh(III) | Schmidt and coworker [6] |
| 2% $Rh/Al_2O_3$ | 300 | 5% $O_2/N_2$ | XPS | Rh(III) | Carpenter [7] |
| | 500 | Air | | Rh(III) | |
| $Rh/Al_2O_3$ | >400 | Air | TPR | $Rh_2O_3$ | Yao et al. [5] |
| Rh/NaY | 400 | Air | TPR | $RhO_2$ | Sachtler and coworkers [8] |
| | 500 | | | $Rh_2O_3$ | |
| $Rh/SiO_2$, $Rh/TiO_2$ | 500 | $O_2$ | $O_2$-volumetric | RhO | Datye and coworkers [3] |
| | >500 | | | $Rh_2O_3$ | |
| $Rh/Al_2O_3$ ($r^a \geq 1.6$ mm) | 500 | $O_2$ | TG/DSC | $RhO_2$ | Yeh and coworker [9] |
| $Rh/Al_2O_3$ ($r<1.1$ nm) | | | | $Rh_2O_3$ | |

[a] Average diameter of rhodium crystallites calculated from 0.90/$D$.

varied with the oxidation temperature, $RhO_2$ prevailed after oxidation at 320°C but $Rh_2O_3$ dominated after calcination at 500°C.

Taylor pointed out in a review [10] that rhodium catalysts tended to deactivate in oxidizing environments at high temperatures. Besides a sintering of rhodium to form large particles [11–13], the deactivation was attributed to the formation of:

1. difficult-to-reduce rhodium oxides [11],
2. a rhodium species interacting strongly with the surface of γ-$Al_2O_3$ support or
3. binary compounds between rhodium oxides and alumina [4,5,14,15].

Many studies [5,14–17] found that catalytic activities of deactivated rhodium catalysts could be partially restored by exposing to reducing environments at temperatures of 600°C or higher. Presumably the activity of rhodium catalysts depends heavily on the chemical environment of $RhO_x$. Therefore, a detailed chemistry on oxidations of rhodium catalysts is needed.

In a previous report [18], we distinguished different species of platinum oxides, i.e., PtO, $PtO_2$ and those incorporated into alumina support, on $Pt/Al_2O_3$ samples with the technique of TPR. In this report, we used the same technique to study the variation in chemical environments of rhodium crystallites supported on alumina with the temperature of oxidation treatments.

## 2. Experimental

### 2.1. Calcined samples

Rhodium catalysts of various rhodium loadings were prepared via the incipient wetness technique by impregnating γ-$Al_2O_3$ powders (Merck, surface area=108 $m^2/g$) with an aqueous $RhCl_3$ solution. Obtained slurries were pretreated sequentially with an overnight drying at 110°C and 4 h calcination at 500°C in air before being stored in capped bottles as calcined samples. The loading of rhodium on the calcined samples was determined by the atomic-emission technique using a Perkin-Elemer Sciex Elan 5000 ICP-MS.

The dispersion ($D$, i.e., percentage of atoms exposed to surface) of rhodium crystallites on each sample was estimated gravimetrically from adsorption of dioxygen ($2.5\times10^4$ Pa) at 25°C under the assumption that a monolayer chemisorption of oxygen atom on rhodium surface has a stoichiometry of $N_o/N_{Rh}s=1$ [9]. The amount of oxygen uptake was monitored in a Setaram TG/DSC 111 dual port calorimeter equipped with a sensitive (±0.25 μg) balance. A detailed description of this system has been given in a previous report [19]. Obtained dispersions of rhodium on the calcined samples are listed in Table 2.

Table 2
Effects of rhodium dispersion and reoxidation temperature ($T_o$) on the TPR characterization on $Rh/Al_2O_3$ samples

| Sample | Dispersion $N_o^{ad}/N_{Rh}$ | $T_o$ (°C) | TPR | |
|---|---|---|---|---|
| | | | $N_o/N_{Rh}$ | Dominant $RhO_x$ |
| 0.9% $Rh/Al_2O_3$ | 1.00 | −30 | 0.93 | $Rh^sO$, $RhO_x$ |
| | | 25 | 1.13 | $RhO_x$, $Rh^iO_x$ |
| | | 100 | 1.23 | $RhO_x$, $Rh^iO_x$ |
| | | 300 | 1.32 | $Rh^iO_x$ |
| | | 500 | 1.22+0.09 | $Rh^iO_x$, Rh aluminate |
| | | 800 | 0.18+1.06 | $Rh^iO_x$, Rh aluminate |
| | | 300[a] | 1.23 | $RhO_x$, $Rh^iO_x$ |
| 3.3% $Rh/Al_2O_3$ | 0.55 | −30 | 0.34 | $RhO^c$, $Rh^sO$ |
| | | 25 | 0.54 | $RhO^c$, $Rh^sO$ |
| | | 100 | 0.95 | $Rh^sO$, $RhO_x$ |
| | | 300 | 1.00 | $RhO_x$ |
| | | 400 | 1.38 | $RhO_x$, $Rh^iO_x$ |
| | | 500 | 2.20 | $RhO_x$, $Rh^iO_x$ |
| | | 700 | 2.01+0.11 | $RhO_x$, $Rh^iO_x$ |
| | | 800 | 1.56+0.51 | $Rh^iO_x$, Rh aluminate |
| 23% $Rh/Al_2O_3$ | 0.18 | −30 | 0.12 | $RhO^c$ |
| | | 25 | 0.18 | $RhO^c$, $Rh^sO$ |
| | | 100 | 0.29 | $RhO^c$, $Rh^sO$ |
| | | 300 | 0.64 | $Rh^sO$ |
| | | 500 | 1.40 | $Rh^sO$, $RhO_x$ |
| | | 700 | 1.29+0.03 | $RhO_x$, $Rh^iO_x$ |
| | | 800 | 1.27+0.12 | $Rh^iO_x$, Rh aluminate |

$N_o^{ad}$: Uptake of oxygen atom measured gravimetrically at 25°C.
[a] A second TPR for 300°C reoxidized sample.

### 2.2. Reoxidized samples

For TPR characterizations, each calcined sample was prereduced for 1 h in flowing hydrogen gas at 400°C and a subsequent purge for 1 h in flowing helium gas (purity of 99.9999%) at 500°C. 0.15 g of reduced $Rh/Al_2O_3$ sample was then reoxidized for 1 h in a flow of 5 vol% $O_2$ in He at a predetermined oxidation temperature ($T_o$) to convert rhodium crystallites into rhodium oxides. Each reoxidized sample was then cooled in pure He for subsequent TPR characterizations.

The TPR study was performed in an apparatus described in a previous report [20]. A 30 ml/min flow of 10 vol% $H_2$ in Ar was used as the reduction gas in TPR experiments. The rate of hydrogen consumption was monitored by a thermal conductivity detector (TCD) when the sample temperature was raised from −60°C to 1000°C at a constant rate of 7°C/min. The amount of oxygen atoms ($N_o$) reduced in TPR experiments was calibrated with the hydrogen consumption. Calculated $N_o/N_{Rh}$ ratios (where $N_{Rh}$ denotes the number of rhodium atoms in each sample) were also listed in Table 2. The software for peak analysis was provided by Scientific Information Service Corporation (SISC).

## 3. Results and discussion

### 3.1. Effects of chloride ions on the reduction of $Rh/Al_2O_3$

The Rh species on calcined samples may be tentatively regarded as a mixture of $RhO_x$ and $RhO_yCl_z$ because they were prepared from $RhCl_3$ precursor and calcined 500°C. Fig. 1 displays TPR traces from three calcined samples with different Rh loadings. Two

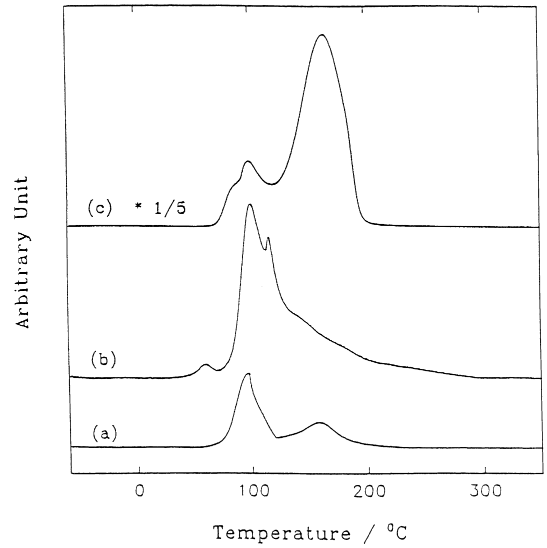

Fig. 1. TPR spectra for reduction of $RhO_x$ and $RhO_yCl_z$ species on calcined samples of $Rh/Al_2O_3$: (a) 0.9% $Rh/Al_2O_3$; (b) 3.3% $Rh/Al_2O_3$; (c) 23% $Rh/Al_2O_3$.

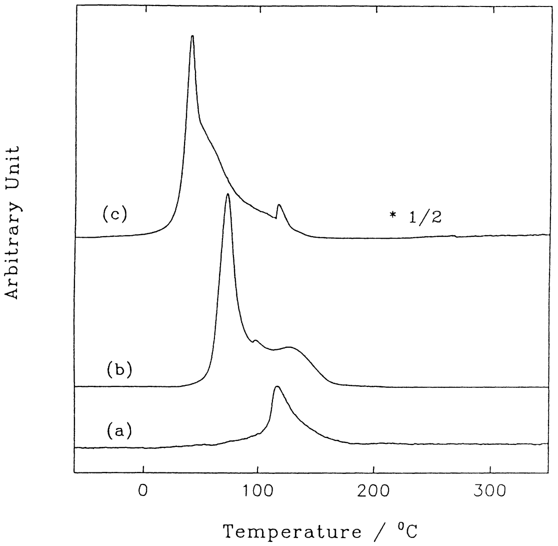

Fig. 2. TPR spectra of $Rh/Al_2O_3$ samples after reoxidation at $T_o$=500°C: (a) 0.9% $Rh/Al_2O_3$; (b) 3.3% $Rh/Al_2O_3$; (c) 23% $Rh/Al_2O_3$.

reduction peaks (at $T_r$~100°C and ~ 170°C, respectively) can be distinguished from these traces. These two peaks may be regarded as the following reductions:

$$RhO_x + xH_2 \rightarrow Rh + xH_2O \qquad (2)$$

$$RhO_yCl_z + \left(y + \frac{z}{2}\right)H_2 \rightarrow Rh + yH_2O + zHCl \qquad (3)$$

The coordinated chloride ions in the $RhO_yCl_z$ complex might be completely removed from rhodium at the termination of TPR reduction (350°C) [18]. The rhodium crystallites reduced may be further converted into rhodium oxide ($RhO_x$) by reoxidation with oxygen:

$$Rh + \frac{x}{2}O_2 \rightarrow RhO_x \qquad (4)$$

Fig. 2 shows TPR characterizations of the three TPR reduced $Rh/Al_2O_3$ samples reoxidized at 500°C. Only a single reduction peak was observed in each sample for the $RhO_x$ species formed at the 500°C reoxidation. The reduction temperatures ($T_r$) of this peak are always lower than 120°C. A comparison of these TPR traces with those in Fig. 1 reveals that the peaks with $T_r$>150°C in Fig. 1 can be assigned to the reduction of $RhO_yCl_z$ species (reaction 3) while the chloride-free $RhO_x$ species formed in reaction 2 generally gives a peak at $T_r \leq 120$°C. The main peak ($T_r$=100°C), the small peaks at $T_r$=60°C and 120°C in Fig. 1(b) and the shoulder at $T_r$=85°C in Fig. 1(c) found in the calcined samples came from reductions of rhodium oxide species in different chemical environments, which will be discussed at Section 3.2 in detail. Obviously, the coordinated chloride ions in $RhO_yCl_z$ complex inhibited the reduction of rhodium ions and these chloride ions can, indeed, be removed from rhodium upon the prereduction treatment at 400°C. Interestingly, the $RhO_x/RhO_yCl_z$ ratio obtained in Fig. 1 varied with the Rh loading. Large $RhCl_3$ particles on a highly loaded $Rh/Al_2O_3$ sample are probably more difficult to convert into $RhO_x$ compared with small $RhCl_3$ particles upon a 500°C calcination. Similar chloride effects have also been found previously from $Pt/Al_2O_3$ systems [18,21].

Fig. 2 indicates that TPR traces for $RhO_x$ supported on alumina vary significantly with the rhodium loadings. Observed variations may be caused by different extent of interaction between these $RhO_x$ species and the $Al_2O_3$ support (rhodium clusters deposited on a lowly loaded $Rh/Al_2O_3$ sample should have a high dispersion and, accordingly, an intimate interaction with the alumina support). Accordingly, effects of

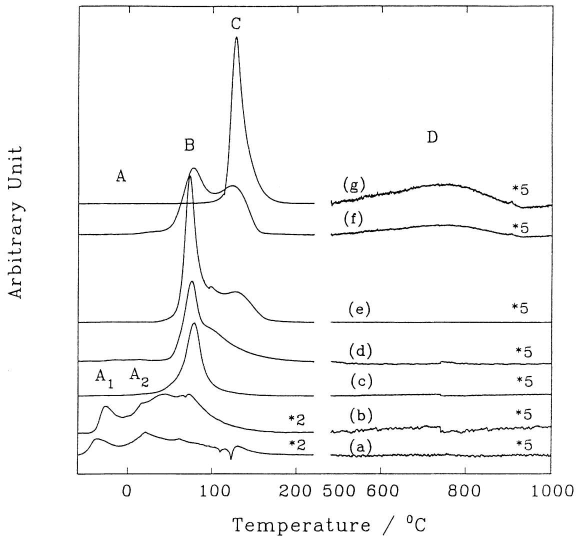

Fig. 3. TPR spectra of 3.3% $Rh/Al_2O_3$ sample after reoxidation at $T_o$: (a) 25°C; (b) 100°C; (c) 300°C; (d) 400°C; (e) 500°C; (f) 700°C; (g) 800°C.

oxidation treatment on the extent of $RhO_x$–$Al_2O_3$ interaction were subsequently examined.

### 3.2. *Effects of oxidation temperature on the reduction of reoxidized samples*

Fig. 3 presents TPR traces obtained from several portions of a prereduced 3.3 wt% $Rh/Al_2O_3$ sample reoxidized at different oxidation temperatures ($T_o$). These traces are composed mainly of four peaks tentatively designated as peaks A ($T_r$ between −30°C and 25°C), B ($T_r$~80°C), C ($T_r$~120°C) and D ($T_r$~750°C), respectively. The existence of these four peaks suggests that reoxidized Rh atoms have at least four different chemical environments.

Relative areas of these four peaks varied with $T_o$ as shown in Fig. 3. Peak A was the dominant reduction signal from the 3.3% $Rh/Al_2O_3$ sample reoxidized at $T_o$=25°C [trace (a) of Fig. 3]. The total peak area of this trace indicates that $RhO_x$ formed on this oxidation treatment has a $N_o/N_{Rh}$ ratio=0.54. This low uptake stoichiometry suggests that the oxygen uptake at room temperature might be limited to an oxygen species on the surface of reduced rhodium crystallites. Peak A is therefore assigned to reductions of an oxide layer formed on the surface of rhodium crystallites ($RhO_s$) upon the oxygen chemisorption. This oxide layer has already been assigned to the β-state species in literature based on TPD of oxygen from single crystals of rhodium [22–24].

Some studies [25–27] have found that structural reconstructions, such as "doubling-step" to "singling-step" transformation, might occur on surfaces of metallic single crystal during extensive oxygen chemisorptions. Such mild reconstruction probably converted part of the oxygen-chemisorbed rhodium system ($RhO_c$) into an oxide structure on metal surface ($Rh_sO$). The broad A peaks in traces (a) and (b) of Fig. 3 may thus reflect the existence of surface oxygen atoms in two different environments, a chemisorption state ($A_1$) at $T_r$=−30°C and a surface oxide state ($A_2$) at $T_r$=25°C.

Since the structural reconstruction is an activated process, the extent of surface reconstruction can be decreased by lowering the oxidation temperature. A chemisorption of dioxygen at $T_o$=−30°C was therefore performed on a reduced 3.3% $Rh/Al_2O_3$ sample. $T_o$ our satisfaction, the TPR trace of this sample reoxidized at this low temperature displayed a big $A_1$ peak and a small $A_2$ peak [trace (a) in Fig. 4].

As the $T_o$ was raised, oxygen atoms on the metal oxide surface might diffuse into the bulk of rhodium

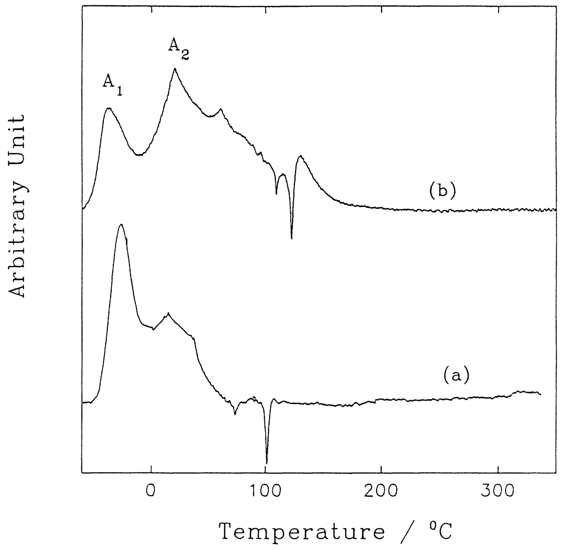

Fig. 4. TPR spectra of 3.3% $Rh/Al_2O_3$ sample after reoxidation at $T_o$: (a) −30°C; (b) 25°C.

crystallites. Peak B (with a $T_r$=80°C) became the major signal when the reduced $Rh/Al_2O_3$ sample was reoxidized at 300°C [trace (c) in Fig. 3]. A chemical stoichiometry of $N_o/N_{Rh}$=1.00 (Table 2) calculated from the peak area indicates that the oxide species formed at $T_o$=300°C should be the bulk crystallites of $RhO_x$. The $x$ is a stoichiometry between 0.5 and 2.0.

Besides the peaks B and C (with a $T_r$=120°C) became an additional dominant peak on raising $T_o$ from 300°C to 500°C [traces (d) and (e) in Fig. 3]. On comparing to results of Fig. 2, the difference in $T_r$ between peaks B and C probably resulted from $RhO_x$ species with different extent of interaction with $Al_2O_3$. Peak B comes from a $RhO_x$ species insignificantly affected by the support while peak C may be assigned to another $RhO_x$ species intimately interacting with the $Al_2O_3$ surface. The interacting species is designated in this report as $Rh_iO_x$ to distinguish from the $RhO_x$ species of peak B. The extent of this surface interaction increased with the $T_o$ of the oxidation treatment (Fig. 3). The $N_o/N_{Rh}$ ratio of $RhO_x$ and $Rh_iO_x$ also increased with $T_o$ (from the ratio 1.00 to 2.20). The deviation of the observed $N_o/N_{Rh}$ ratio from the stoichiometric values of 1.0, 1.5 or 2.0 reflected that a mixture of RhO, $Rh_2O_3$ or $RhO_2$ existed on these reoxidized samples.

The reoxidation of a reduced $Rh/Al_2O_3$ sample above 700°C caused a dramatically environmental change to the oxidized $RhO_x$. Peak D ($T_r$=750°C) became a noticeable signal in TPR traces (f) and (g) in Fig. 3. This high $T_r$ peak indicated that the chemical stability of this $RhO_x$ species was rather high. Since $MAl_2O_4$ spinel species have been reported in many alumina-supported metal samples (including Pt [18], Co [28], Ni [29,30], Cu [31] and Pd [32]) upon high temperature calcination treatments, and all these $MAl_2O_4$ species display a much higher $T_r$ temperature than their corresponding metal oxide species, peak D is therefore assigned to the reduction of $Rh(AlO_2)_y$ species. This species was formed by diffusion of rhodium oxides into sublayers of the $Al_2O_3$ structure at high oxidation temperatures. The formation of $Rh(AlO_2)_y$ has been regarded as one of the major reasons for the deactivation of $Rh/Al_2O_3$ catalysts towards many oxidation reactions [4,5,14,15].

Fig. 5 presents a model for the extent of interaction between dioxygen and rhodium crystallites supported on alumina. On increasing the interaction temperature, $RhO_C$ ($T_o$∼ −30°C), $Rh_sO$ ($T_o$ ∼25°C), $RhO_x$ ($T_o$∼300°C), $Rh_iO_x$ ($T_o$∼500°C) and $Rh(AlO_2)_y$ ($T_o$∼800°C) alternate becoming dominant oxidized products on the 3.3% $Rh/Al_2O_3$ sample.

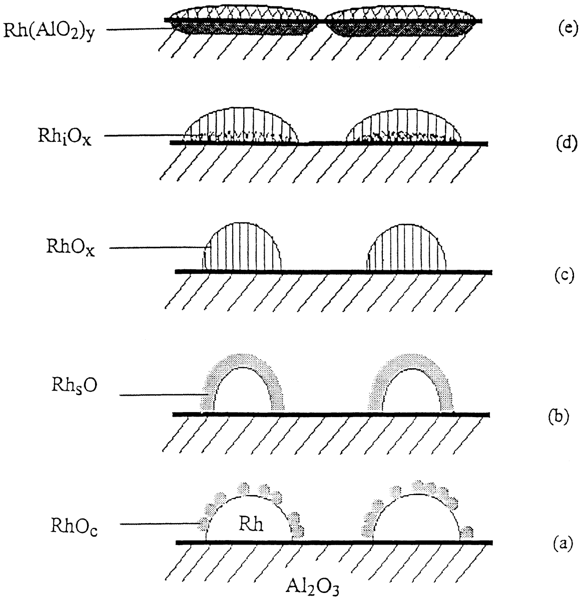

Fig. 5. The extent of interaction between dioxygen and rhodium crystallites supported on alumina for 3.3% $Rh/Al_2O_3$ sample at $T_o$: (a) < −30°C; (b) 50°C; (c) 300°C; (d) 500°C; (e) 800°C.

### 3.3. *Effects of rhodium loading on TPR of reoxidized $Rh/Al_2O_3$*

All five rhodium oxide species, i.e., $RhO_C$, $Rh_SO$, $RhO_x$, $Rh_iO_x$ and $Rh(AlO_2)_y$, distinguished from the 3.3 wt% $Rh/Al_2O_3$ sample, appeared also in the TPR traces (Fig. 6) of reoxidized 23% $Rh/Al_2O_3$ samples. However, the following three major variations have been found on this low dispersion rhodium sample (average diameter ∼5 nm or dispersion=18%)

1. Chemisorbed oxygen ($RhO_c$) is the only species at $T_o \leq 25$°C.
2. $T_o$ required for the formation of an oxide surface ($Rh_sO$) through surface reconstruction was increased to 300°C (comparing traces (a)–(d) of Fig. 6 with Fig. 4).
3. Temperature required for the formation of $RhO_x$ (peak B) and $Rh_iO_x$ (peak C) species was increased to $T_o \geq 500$°C.

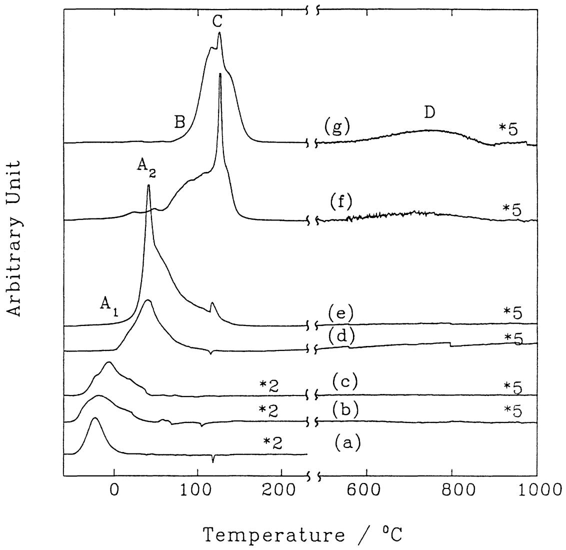

Fig. 6. TPR spectra of 23% $Rh/Al_2O_3$ sample after reoxidation at $T_o$: (a) −30°C; (b) 25°C; (c) 100°C; (d) 300°C; (e) 500°C; (f) 700°C; (g) 800°C.

Evidently, a high oxidation temperature is generally required for the formation of deep oxidized species on this lowly dispersed rhodium sample.

Fig. 7 shows TPR traces of 0.9 wt% $Rh/Al_2O_3$ ($D$=100%) reoxidized at different $T_o$. The highly dispersed rhodium crystallites on this sample have been fully reoxidized to bulk $RhO_x$ even at the room temperature (trace (b) of Fig. 7). The finely dispersed bulk rhodium-oxides also easily spread over onto the alumina surface (trace (e) of Fig. 7) and diffused into the support structure (trace (f) of Fig. 7).

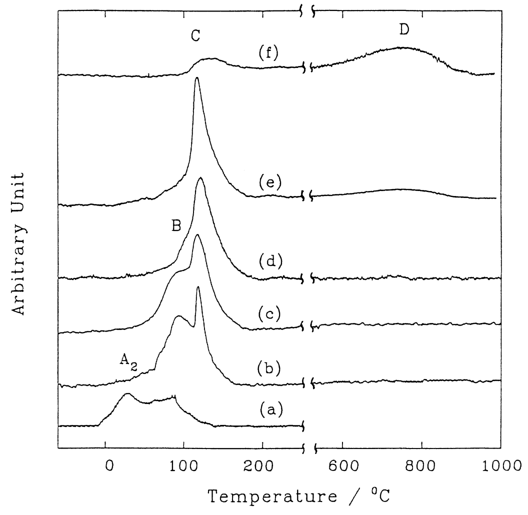

Fig. 7. TPR spectra of 0.9% $Rh/Al_2O_3$ sample after reoxidation at $T_o$: (a) −30°C; (b) 25°C; (c) 100°C; (d) 300°C; (e) 500°C; (f) 800°C.

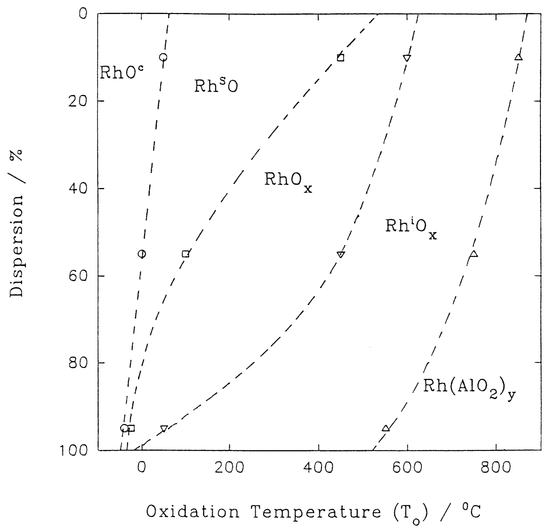

Fig. 8. Phase diagram for the variation of rhodium oxide species on the dispersion of rhodium samples and the reoxidation temperatures ($T_o$). The marked phase in each region indicates only the dominant phase among them. Dotted line used to separate different oxide phases because there existed a mixture of two or more phases.

The type of rhodium oxide species formed during the oxidation therefore varies with both the $T_o$ temperature and the rhodium dispersion. Fig. 8 presents a phase diagram for the variation of rhodium oxide species on these two factors. Dotted lines are used in this diagram to separate different oxide phases because a mixture of two or more phases is generally found and the marked phase in each region indicates only the dominant phase among them.

### 3.4. *Reduction of $Rh(AlO_2)_y$*

The finely dispersed bulk rhodium-oxides on the 0.9% $Rh/Al_2O_3$ sample diffuse easily into the structure of alumina support at severe oxidation condition. Trace (a) in Fig. 9 showed that the $Rh(AlO_2)_y$ species was the dominant rhodium phase at $T_o$=800°C. Rhodium atoms in the $Rh(AlO_2)_y$ structure have been proposed to be catalytically inactive [4,5,14–17]

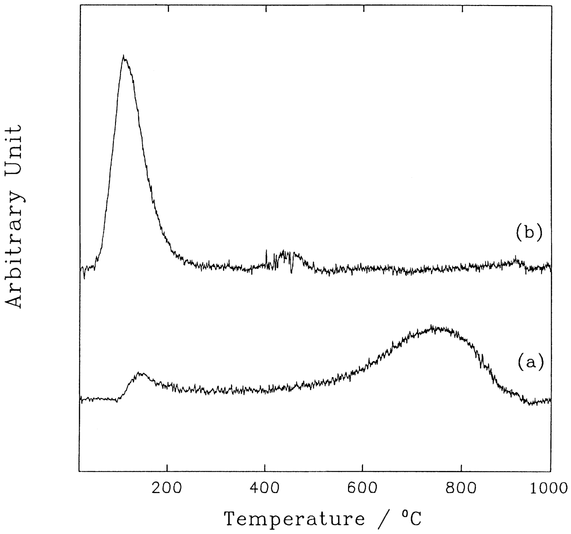

Fig. 9. TPR spectra of: (a) 0.9% Rh/$Al_2O_3$ sample oxidized at 800°C; (b) sample (a) reoxidized at 300°C.

towards oxidation reactions and be able to partially resume their activity by an appropriate reduction treatment (at $T_r$~600°C) [5,15–17]. In order to study whether the rhodium atoms reduced from the $Rh(AlO_2)_y$ species is remained in the alumina structure, the sample reduced in the TPR treatment of trace (a) was therefore subsequently reoxidized mildly at $T_o$=300°C. Trace (b) of Fig. 9 shows the TPR characterization of this reoxidized sample where reductions of $RhO_x$ (peak B) and $Rh_iO_x$ (peak C) were observed Table 3. The $N_o/N_{Rh}$ ratio of these two traces (see Table 2) indicates that the incorporated $Rh(AlO_2)_y$ species can be completely reduced and all of the reduced rhodium would segregate from the $Al_2O_3$ structure back to the surface of alumina upon a severe reduction at $T_r$=750°C. A similar result has also been reported by Mccabe and coworker [4].

Table 3
Reduction temperature of various rhodium species supported on γ-$Al_2O_3$

| Oxide species | Reduction temperature in TPR (°C) |
|---|---|
| $RhO_yCl_z$ | ~170 |
| $RhO_c$ (peak $A_1$) | ~−30 |
| $Rh_sO$ (peal $A_2$) | ~25 |
| $RhO_x$ (peak B) | ~80 |
| $Rh_iO_x$ (peak C) | ~120 |
| $Rh(AlO_2)_y$ (peak D) | ~750 |

## 4. Conclusions

The TPR technique has been successfully used to characterize the oxidized rhodium species on Rh/$Al_2O_3$ samples. In this study, we propose

1. Two kinds of surface oxide [$RhO_c$ ($T_r$=−30°C) and $Rh_sO$ (25°C)], two kinds of bulk oxides [$RhO_x$ (80°C) and $Rh_iO_x$ (120°C)], and an oxide in the alumina support [$Rh(AlO_2)_y$ (750°C)] are sequentially formed (see Fig. 5) on progressive oxidation of reduced Rh/$Al_2O_3$.
2. A phase diagram for the existance of these oxidized species is summarized in Fig. 8. The formation of these species varied with the dispersion of the supported rhodium and the oxidation temperature.
3. The catalytically inactive $Rh(AlO_2)_y$ may segregate completely to actively $RhO_x$ species on a hydrogen reduction at $T_r$>750°C.

## Acknowledgements

The authors would like to thank the National Science Council of the Republic of China for financial support of this manuscript under contract no. NSC 87-2113-M007-007. The second author (Yeh) also wants to thank the state key laboratory in $C_1$ chemical technology of the People's Republic of China for a kind visiting professorship to Tsinghua University of Beijing in the autumn of 1997.

## References

[1] W.M.H. Sachtler, Proceedings of the Eighth International Congress on Catalysis, vol. I, Berlin, 1984, p. 151.
[2] A. Munoz, G. Munuera, P. Malet, A.R. Gonzalez-Elipe, T.P. Espinos, Surf. Interfacial Anal. 12 (1988) 247.
[3] A.D. Logan, E.J. Braunschweig, A.K. Datye, D.J. Smith, Ultramicroscopy 31 (1989) 132.
[4] C. Wong, R.W. Mccabe, J. Catal. 119 (1989) 47.
[5] H.C. Yao, S. Japar, M. Shelef, J. Catal. 50 (1977) 407.
[6] T. Wang, L.D. Schmidt, J. Catal. 71 (1981) 411.
[7] J.E. Carpenter, J. Catal. 80 (1983) 472.
[8] S.V. Chunemann, B. Adelman, W.M.H. Sachtler, Catal. Lett. 27 (1994) 259.

[9] C.B. Wang, C.T. Yeh, J. Mol. Catal. 120 (1997) 179.
[10] K.C. Taylor, Automotive Catalytic Converters, Springer, Berlin, 1984.
[11] J.T. Kiss, R.D. Gonzalez, Ind. Eng. Chem. Prod. Res. Dev. 24 (1985) 216.
[12] D.T.C. Yates, E.B. Prestridge, J. Catal. 106 (1987) 549.
[13] R.M.J. Fiedorow, B.S. Chahar, S.E. Wanke, J. Catal. 51 (1978) 193.
[14] H.C. Yao, H.K. Stepien, H.S. Gandhi, J. Catal. 61 (1980) 547.
[15] D. Duprez, G. Delahay, H. Abderrahim, J. Grimblot, J. Chim. Phys. 83 (1986) 465.
[16] D. Duprez, J. Barrault, C. Geron, Appl. Catal. 37 (1988) 105.
[17] J.C. Summers, S.A. Ausen, J. Catal. 58 (1979) 131.
[18] C.P. Hwang, C.T. Yeh, J. Mol. Catal. 112 (1996) 295.
[19] Y.S. Ho, C.B. Wang, C.T. Yeh, J. Mol. Catal. 112 (1996) 287.
[20] T.Y. Chou, C.P. Hwang, C.T. Yeh, J. Thermal Anal. 46 (1996) 305.
[21] H. Lieske, G. Lietz, H. Spindler, J. Volter, J. Catal. 81 (1983) 8.
[22] G.B. Fisher, S.J. Schmieg, J. Vac. Sci. Technol. A 1 (1983) 1064.
[23] A.N. Salanov, V.I. Savchenko, Surf. Sci. 296 (1993) 393.
[24] E. Schwarz, J. Lenz, H. Wohlgemuth, K. Christmann, Vacuum 41 (1990) 167.
[25] L. Niu, D.D. Koleske, D.J. Gaspar, S.F. King, S.J. Sibener, Surf. Sci. 356 (1996) 144.
[26] S.L. Chang, P.A. Thiel, J. Phys. Chem. 88 (1988) 2071.
[27] J.W. May, Adv. Catal. 21 (1970) 244.
[28] H.C. Tung, C.T. Yeh, J. Catal. 122 (1990) 211.
[29] R.P. Sieg, G. Constabaris, R.H. Linquist, American Chemical Society Meeting, New York, 1963.
[30] P. Salagre, J.L.G. Fierro, F. Medina, J.E. Sueiras, J. Mol. Catal. 106 (1996) 125.
[31] S.P. Chen, Effect of adding lanthana and copper on the thermal stability of alumina, MS Dissertation, National Tsing-Hua University, Taiwan, 1992.
[32] T.H. Chang, Solid state DNMR studies on adsorption of deuterium on catalysts of supported noble metals, Ph.D. Dissertation, National Tsing-Hua University, Taiwan, 1990.